The Astronomical Journal, 145:37 (15pp), 2013 February doi:10.1088/0004-6256/145/2/37
© 2013. The American Astronomical Society. All rights reserved. Printed in the U.S.A.

THE INITIAL MASS FUNCTION AND THE SURFACE DENSITY PROFILE OF NGC 6231

Hwankyung Sung[1,4], Hugues Sana[2], and Michael S. Bessell[3]
[1] Department of Astronomy and Space Science, Sejong University, 98, Kunja-dong, Kwangjin-gu, Seoul 143-747, Republic of Korea; sungh@sejong.ac.kr
[2] Astronomical Institute "Anton Pannekeok," Amsterdam University, Science Park 904, 1098-XH Amsterdam, The Netherlands; H.Sana@uva.nl
[3] Research School of Astronomy and Astrophysics, Australian National University, MSO, Cotter Road, Weston, ACT 2611, Australia; bessell@mso.anu.edu.au
Received 2012 October 21; accepted 2012 November 16; published 2013 January 10

ABSTRACT

We have performed new wide-field photometry of the young open cluster NGC 6231 to study the shape of the initial mass function (IMF) and mass segregation. We also investigated the reddening law toward NGC 6231 from optical to mid-infrared color excess ratios, and found that the total-to-selective extinction ratio is $R_V = 3.2$, which is very close to the normal value. But many early-type stars in the cluster center show large color excess ratios. We derived the surface density profiles of four member groups, and found that they reach the surface density of field stars at about 10′, regardless of stellar mass. The IMF of NGC 6231 is derived for the mass range 0.8–45 $M_\odot$. The slope of the IMF of NGC 6231 ($\Gamma = -1.1 \pm 0.1$) is slightly shallower than the canonical value, but the difference is marginal. In addition, the mass function varies systematically, and is a strong function of radius—it is very shallow at the center, and very steep at the outer ring suggesting the cluster is mass segregated. We confirm the mass segregation for the massive stars ($m \gtrsim 8\ M_\odot$) by a minimum spanning tree analysis. Using a Monte Carlo method, we estimate the total mass of NGC 6231 to be about $2.6\,(\pm 0.6) \times 10^3\ M_\odot$. We constrain the age of NGC 6231 by comparison with evolutionary isochrones. The age of the low-mass stars ranges from 1 to 7 Myr with a slight peak at 3 Myr. However, the age of the high-mass stars depends on the adopted models and is 3.5 ± 0.5 Myr from the non-rotating or moderately rotating models of Brott et al. as well as the non-rotating models of Ekström et al. But the age is 4.0–7.0 Myr if the rotating models of Ekström et al. are adopted. This latter age is in excellent agreement with the timescale of ejection of the high-mass runaway star HD 153919 from NGC 6231, albeit the younger age cannot be entirely excluded.

Key words: open clusters and associations: individual (NGC 6231) – stars: formation – stars: pre-main sequence

Online-only material: color figures, machine-readable and VO tables

1. INTRODUCTION

The young open cluster NGC 6231 is considered to be the core cluster of the Sco OB1 association (Perry et al. 1990) and is one of the brightest open clusters in the southern hemisphere. Although there is a small amount of differential reddening (Sung et al. 1998; Raboud et al. 1997), the reddening of the inner 10′ region is relatively constant and low. NGC 6231 is a rare case of an exposed young open cluster. In addition, there are about 150 O, B, and A main-sequence (MS) or post-MS stars within 10′ from the center of NGC 6231, and therefore NGC 6231 is a good target for the study of dynamical evolution of open clusters (Raboud & Mermilliod 1998). In most cases there are only a handful of massive O-type stars in nearby open clusters (the Orion Nebula Cluster or NGC 2264) and as a result, the initial mass function (IMF) of the massive part of these clusters inevitably suffers from low-number statistics. NGC 6231 is richer in massive stars than other nearby young open clusters, and is relatively closer and more transparent than young compact clusters such as NGC 3603 (Sung & Bessell 2004). In this respect, NGC 6231 is a good target for the study of the stellar IMF, especially in the massive part.

One of hot issues in cluster research is the origin of mass segregation in open clusters. The failure of the classical approach was well tested in Moeckel & Bonnell (2009), and they concluded that several young open clusters, including the Orion Nebula Cluster and NGC 6231, are too young to be dynamically relaxed. They also concluded that strong primordial mass segregation is unlikely to be dynamically erased over the first few Myr of cluster evolution. The breakthrough in the so-called primordial mass segregation in young open clusters was made by McMillan et al. (2007). They showed that mergers of small clumps, which are initially mass segregated, lead to larger systems that inherit the progenitor clumps' segregation. Allison et al. (2009b, 2010) performed numerical simulations of cool, clumpy clusters, and showed that subvirial, fractal clusters are often dynamically mass segregated on timescales far shorter than that expected from simple dynamical models. Allison et al. (2010) showed that the formation of Trapezium-like massive multiples is highly probable in such a cool, clumpy cluster at a very early phase. They also showed the possibility of ejection of massive stars due to the dynamical interaction between massive stars during the core-collapse phase of the cluster. In addition, Allison et al. (2009a) devised an objective method to calculate the degree of mass segregation based on the minimum spanning tree method. One of the important aims of this work is to study the extent of mass segregation in NGC 6231.

Sung et al. (1998, hereafter SBL98) performed *UBVRI* and Hα photometry and found several pre-main-sequence (PMS) stars and PMS candidates. But the number of PMS stars with Hα emission was far smaller than the number of low-mass PMS stars expected from the number of massive MS and post-MS stars in the cluster. They suggested possible explanations for the deficit of PMS stars with Hα emission, such as past supernova explosions or strong stellar winds from massive stars in the cluster. However, Baume et al. (1999) undertook a statistical approach and showed the nearly normal IMF for the cluster. From analysis of the 180 ks *XMM-Newton* campaign of NGC 6231, Sana et al. (2006) found 610 X-ray sources

[4] Visiting Fellow, Research School of Astronomy and Astrophysics, Australian National University, Weston, ACT 2611, Australia.

in the field of view and confirmed that many of these X-ray sources are bona fide low-mass PMS stars in NGC 6231 (Sana et al. 2007). Recently, Damiani et al. (2009) detected more than 1600 X-ray point sources from the 120 ks *Chandra* ACIS observation, and confirmed the Sana et al. (2007) results. In addition, they analyzed the X-ray spectra of about 500 X-ray sources without optical or near-IR counterparts, and found unusually hard spectra for these sources. These objects could be low-mass PMS stars ($V - I \gtrsim 2.0$) showing high coronal temperatures (see Figure 1 of Sung et al. 2008b).

Another interesting issue for NGC 6231 concerns past supernovae explosions in the cluster. The massive star content, the IMF, and the age of NGC 6231 strongly suggest the likelihood of at least one supernova. Bessell et al. (1974) studied the O6.5Iaf star HD 153919, the optical companion of the X-ray binary, 2U1700-37, and suggested from the reddening and brightness of the star, that it may be at the same distance as Sco OB1. Later Ankay et al. (2001) suspected that Sco OB1 may be the origin of this runaway high-mass X-ray binary using the high-quality proper motion data from *Hipparcos*. From the optical polarization observation of 35 stars in the cluster, Feinstein et al. (2003) found a curious semicircular pattern of polarization angles of some stars in the center of NGC 6231. They interpreted it as a fingerprint of a past supernova explosion. But they seem not to have realized the existence of the runaway high-mass X-ray binary HD 153919. Alternatively, Black et al. (2008) proposed the semicircular pattern of polarization angles as the remnants of the historical nova in 1437 recorded in the old Korean Veritable Records of King Sejong *Sejong Sillok*.

Raboud (1996) studied the binary frequency of B-type stars in NGC 6231 and derived a minimum fraction of 52%. Recently, Sana et al. (2008) studied the binary fraction of O-type stars in the cluster and obtained a minimum fraction of 0.63. The fraction of binaries, as well as the mass ratio in binary systems, could be very important subjects of study (see Sana et al. 2012) because we still have insufficient information on the mass function of secondaries in binary systems (see Weidner et al. 2009 for its influence on the mass function). In this respect NGC 6231 could be a good target because it is relatively closer and therefore it is easy to obtain high-quality spectra with medium-size telescopes.

New wide-field *UBVI* and Hα photometry of NGC 6231 is presented and compared in Section 2. Based on the new photometric data, several photometric diagrams are presented in Section 3. The reddening law toward NGC 6231, reddening, distance, and surface density profiles are also derived in Section 3. The Hertzsprung–Russell diagram (HRD) of NGC 6231 is constructed in Section 4. The IMF and age of NGC 6231 is derived from the HRD by comparing the observed data and stellar evolution models in this section. The mass segregation in NGC 6231 is investigated in the same section. Discussion on the runaway O6.5Iaf star HD 153919 and the origin of mass segregation is presented in Section 5. The summary is in Section 6.

2. OBSERVATIONS AND DATA REDUCTION

UBVI and Hα CCD photometry of NGC 6231 was performed on 2000 June 22 (NW and SW regions) and 25 (NE and SE regions) at Siding Spring Observatory with the 40 inch (1 m) telescope ($f/8$) and a thinned SITe 2048 $\times$ 2048 CCD (24 μm pixels). The filters used were the same as those used for the observation of NGC 2244 (Park & Sung 2002). Two sets of exposure times were used in the observations—long: 60 s in I, 150 s in V, 300 s in B, 600 s in U and Hα—and short: 2 s in I and V, 3 s in B, 30 s in U and Hα. The seeing was good on 2000 June 25 (about 1$''$.4 in V long-exposed images), but was bad on 2000 June 22 (2$''$.2–3$''$.2). The seeing strongly affects the photometry of faint stars—completeness and limiting magnitude. The limiting magnitude in V on 2000 June 22 ($V_{\rm limit} \approx 20.5$ mag) is more than 0.5 mag brighter than that on 2000 June 25 ($V_{\rm limit} \gtrsim 21.0$ mag).

All the preprocessing, such as the overscan correction, bias subtraction, and flat fielding, was done using the IRAF/CCDRED package. Instrumental magnitudes were obtained using IRAF/DAOPHOT via point spread function fitting for the target images and via simple aperture photometry for standard stars. All the instrumental magnitudes were transformed to the standard *UBVI* system using SAAO E-region standard stars, E5 (E5-R, -O, -T), E6 (E6-U, 61, -Y, -W), and E7 (E7-W, 37, -c, -X; see Sung & Bessell 2000 for details). We observed E5 (and E7 on 2000 June 25) region(s) twice at high (airmass $\approx$1.1) and low altitude (airmass $\approx$2.0) to determine the atmospheric extinction coefficients and the time variation coefficients accurately. The primary extinction coefficients, time variation coefficients of the photometric zero points (unit: magnitude per hour—see Equations (1)–(4) in Sung et al. 2008a), and photometric zero points at midnight were derived from standard star photometry, and listed in Table 1. On 2000 June 22, the time variation was a function of wavelength, largest in U but zero in I. On 2000 June 25, the time variation in UBV had similar values, but in I it had the opposite sign. The secondary extinction coefficients for U and B were adopted from the mean values used in Sung & Bessell (2000). Although there were no standard magnitudes in Hα, we transformed Hα to R (i.e., pseudo-R) so as to calculate the Hα index (Sung et al. 2000; Park & Sung 2002).

A total of 27,325 stars were measured in about a 40$'$ $\times$ 40$'$ area centered on NGC 6231, and are presented in Table 2. For 12 stars in Table 2 that were saturated in our images we have substituted data from SIMBAD,[5] WEBDA[6] (open cluster database), or SBL98. Data for some stars missed in the new photometry were taken from SBL98. These data are marked with an "*" after the identification number in the first column. We also listed Two Micron All Sky Survey (2MASS) identification of the objects in the 2MASS point source catalog (Skrutskie et al. 2006) in the 16th column. The optical counterparts of X-ray sources (Sana et al. 2006) are identified, and marked as "X" (the closest or the only objects within the search radius of 3$''$.5) or "x" (star within 3$''$.0, but second-closest star). We also identified Hα emission stars (see Section 3.1), and these are marked as "H" (strong Hα emission stars) or "h" (weak Hα emission candidates). The membership information is in the 17th column. A total of 522 X-ray emission stars ("X" in Column 17) and 70 X-ray emission candidates ("x") are identified among 610 X-ray sources (Sana et al. 2006). Among them, 11 stars are X-ray emission stars with Hα emission ("+"), and 7 stars are X-ray emission stars with weak Hα emission ("−"). Other information such as duplicity, variability, ID in SBL98, spectral type, and other identifications are listed in subsequent columns. The finder chart based on the new photometry is shown in Figure 1.

The *UBVI* magnitude and colors from this photometry were compared with the previous photoelectric and CCD photometry in Table 3. Although the agreement in zero points was quite good, the scatter was somewhat large because most photoelectric

[5] http://simbad.u-strabg.fr/simbad
[6] http://www.univie.ac.at/webda/

Table 1
Standard Stars, Atmospheric Extinction Coefficients, Time Variation Coefficients, and Photometric Zero Points

Date of Observations	Standard Stars	Filter	Extinction Coefficients	Time Variation	Photometric Zero Points[a]
		I	0.101 ± 0.007	0.000	22.285 ± 0.011
	E5-R[b], E5-O[b], E5-T[b]	V	0.182 ± 0.004	-0.0014 ± 0.0008	22.791 ± 0.009
2000 Jun 22	E6-U, E661, E6-Y, E6-W	B	0.294 ± 0.007	-0.0035 ± 0.0016	22.640 ± 0.011
	E7-W, E737, E7-c, E7-X	U	0.533 ± 0.016	-0.0056 ± 0.0034	20.213 ± 0.022
		Hα	0.101 ± 0.017	...	18.067 ± 0.024
		I	0.070 ± 0.006	$+0.0063^{c} \pm 0.0011$	22.284 ± 0.008
	E5-R[b], E5-O[b], E5-T[b]	V	0.134 ± 0.005	$-0.0048^{c} \pm 0.0014$	22.760 ± 0.008
2000 Jun 25	E6-U, E661, E6-Y, E6-W	B	0.271 ± 0.006	$-0.0041^{c} \pm 0.0014$	22.622 ± 0.009
	E7-W[b], E737[b], E7-c[b], E7-X[b]	U	0.506 ± 0.012	$-0.0044^{c} \pm 0.0014$	20.193 ± 0.018
		Hα	0.092 ± 0.010	...	18.072 ± 0.003

Notes.
[a] Photometric zero points at midnight.
[b] Observed twice—once at meridian, the other at airmass ≈2.
[c] For UT $\leqslant 13^{h}$.

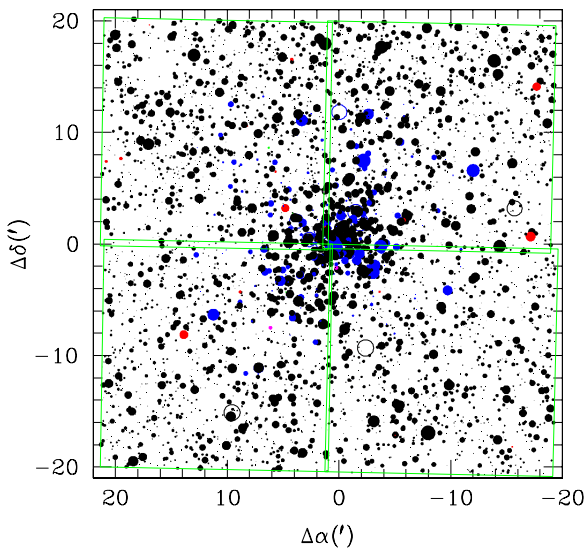

Figure 1. Finder chart of NGC 6231 for the stars brighter than $V = 17$. The size of the dots is proportional to the brightness of the star. Large open circles represent the position of bright stars (data from SIMBAD database). The position of stars is relative to the adopted center of NGC 6231 (α(J2000) = $16^{h}54^{m}11\overset{s}{.}70$, δ(J2000) = $-41°50'20\overset{''}{.}3$). Large squares represent four fields of view of the SSO SITe 2048 × 2048 CCD.

(A color version of this figure is available in the online journal.)

photometric studies were limited to bright stars and many of these bright stars are variables or optical doubles. We compared our new data with SBL98 along with the relevant colors in Figure 2. The major difference between the two sets of data was in the standard stars used. Our new photometry, relative to SBL98, was slightly brighter in V and slightly bluer in $B-V$ for redder stars. Our new $V-I$ was slightly redder, but with no evident color dependency. For $U-B$, although the average difference is close to zero, there was a strong color dependency. Such a difference is caused by the nonlinear correction term in the transformation to the Landolt's U system (see Sung & Bessell 2000 for details) which is related to the size of the Balmer jump. In this respect (see the bottom panel of Figure 2) we can understand the difference between our new $U-B$ and those from photoelectric photometry, i.e., most stars observed with photoelectric photometry are brighter and bluer, and therefore our new $U-B$ is slightly bluer for blue stars.

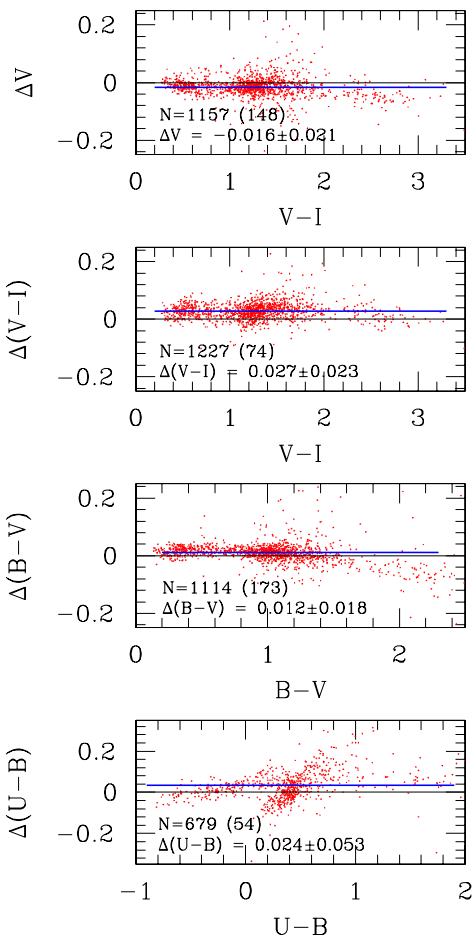

Figure 2. Comparison of the photometry. The difference Δ is in the sense of our new photometry minus Sung et al. (1998) for $V \leqslant 17$ mag (V, $V-I$, and $B-V$) and $V \leqslant 16$ mag ($U-B$). Our new photometry is slightly brighter in V, slightly redder in $V-I$ and $B-V$, but systematically bluer in $B-V$ for red stars. The difference in $U-B$ is somewhat larger and nonlinear. See the text for details.

(A color version of this figure is available in the online journal.)

3. PHOTOMETRIC DIAGRAMS AND SURFACE DENSITY PROFILES

3.1. Color–Color Diagrams and Reddening

The color–color diagrams of the stars in the observed region are shown in Figure 3. X-ray emission stars and Hα emission

Table 2
Photometric Data[a]

ID	α_{J2000}	δ_{J2000}	V	$V-I$	$B-V$	$U-B$	ϵ_V	ϵ_{V-I}	ϵ_{B-V}	ϵ_{U-B}	N_{obs}				2MASS	M[b]	D/V[c]	SBL98	Sp	Remark
3610	16:54:17.95	−41:48:01.6	11.063	0.355	0.210	−0.492	0.001	0.002	0.008	0.005	2	2	2	2	16541793-4148013			480	B2IVn	Se213
3611	16:54:17.96	−41:44:57.1	16.460	1.256	1.060	0.654	0.000	0.002	0.004	0.021	4	4	3	2	16541795-4144568			6777		
3612	16:54:17.97	−42:00:37.3	17.808	1.717	1.345	0.809	0.013	0.027	0.026	0.108	1	1	1	1	16541794-4200373					
3613	16:54:17.98	−42:09:07.4	12.898	0.843	0.650	0.129	0.000	0.003	0.001	0.003	3	3	3	4						
3614	16:54:17.98	−41:31:22.8	16.849	1.311	1.049	0.496	0.019	0.020	0.022	0.036	2	2	1	1	16541799-4131229					
3615	16:54:17.99	−41:56:12.5	17.182	1.592	1.250	0.651	0.001	0.002	0.017	0.060	2	2	1	1	16541798-4156125			6779		
3616	16:54:18.01	−41:32:47.3	17.420	2.991	2.393	...	0.005	0.014	0.054	...	2	2	1	0	16541801-4132474					
3617	16:54:18.01	−41:59:12.7	17.577	1.667	1.334	0.873	0.022	0.029	0.027	0.081	2	2	1	1	16541798-4159126			6781		
3618	16:54:18.03	−41:45:11.8	14.154	0.907	0.670	0.381	0.007	0.006	0.005	0.005	4	4	4	3	16541802-4145117			481		Se188
3619	16:54:18.17	−41:48:13.0	17.542	1.414	1.273	...	0.000	0.011	0.030	...	2	2	1	0	16541819-4148125			6790		
3620	16:54:18.17	−41:50:16.9	13.065	0.572	0.370	−0.040	0.002	0.007	0.012	0.000	3	3	3	3	16541814-4150164			482	B9V	Se225
3621	16:54:18.18	−41:53:36.9	13.337	0.608	0.420	0.105	0.011	0.012	0.011	0.003	2	2	2	2	16541819-4153372			483		
3622	16:54:18.19	−41:45:33.1	12.094	2.350	1.865	2.328	0.001	0.017	0.006	0.011	3	2	3	2	16541820-4145330			484		
3623	16:54:18.22	−41:33:59.2	16.877	1.218	0.971	0.470	0.005	0.011	0.009	0.045	2	2	2	1	16541823-4133592					
3624	16:54:18.27	−41:34:12.0	13.276	0.568	0.384	0.229	0.003	0.005	0.005	0.008	2	2	2	2	16541828-4134120					
3625	16:54:18.29	−41:50:10.1	17.168	1.827	...	...	0.061	0.052	...	...	2	2	0	0	16541824-4150097			6792		
3626	16:54:18.29	−41:51:35.2	9.597	0.360	0.181	−0.684	0.007	0.012	0.009	0.007	1	1	1	1	16541832-4151357		V	486	B1V(n)	Se238,HD 326330, bCep
3627	16:54:18.30	−41:46:38.3	14.640	1.855	1.629	1.696	0.015	0.002	0.003	0.019	4	4	4	2	16541828-4146381			485		Se204
3628	16:54:18.33	−41:32:23.7	8.454	0.234	0.116	−0.456	0.016	0.038	0.024	0.018	1	1	1	1	16541837-4132240				B9Ib-II	HD 152269
3629	16:54:18.34	−41:45:00.0	17.447	1.646	1.258	0.711	0.022	0.001	0.005	0.147	3	3	2	2	16541832-4144599			6800		
3630	16:54:18.37	−41:35:23.0	17.462	1.440	1.175	0.918	0.008	0.050	0.013	0.082	2	2	1	1	16541836-4135228					

Notes.
[a] Units of right ascension are hours, minutes, and seconds of time, and units of declination are degrees, arcminutes, and arcseconds.
[b] Membership: X: X-ray emission star; H: Hα emission star; h: Hα emission candidate; +: X + H; −: X + h.
[c] Duplicity or variability: D: stars whose PSF shows a double, but measures as a single star; V: variable from the literature, variable types if available noted in the last column (dSct: δ Scuti type variable, bCep: β Cephei type variable).

(This table is available in its entirety in machine-readable and Virtual Observatory (VO) forms in the online journal. A portion is shown here for guidance regarding its form and content.)

Table 3
Comparison with Photoelectric and CCD Photometry

Author	ΔV	$n(n_{ex})^a$	$\Delta(V-I)$	$n(n_{ex})^a$	$\Delta(B-V)$	$n(n_{ex})^a$	$\Delta(U-B)$	$n(n_{ex})^a$
Bok et al. (1966)	-0.022 ± 0.053	10 (2)	...	...	$+0.009 \pm 0.023$	12 (0)	-0.027 ± 0.045	11 (1)
Feinstein & Ferrer (1968)	$+0.025 \pm 0.132$	7 (1)	...	...	$+0.017 \pm 0.041$	7 (1)	-0.054 ± 0.061	7 (1)
Seggewiss (1968)	-0.017 ± 0.051	24 (1)	...	...	$+0.007 \pm 0.068$	23 (1)	$+0.012 \pm 0.091$	23 (1)
Schild et al. (1969)	-0.024 ± 0.017	16 (1)	...	...	-0.003 ± 0.014	16 (1)	-0.003 ± 0.030	17 (0)
Garrison & Schild (1979)	-0.007 ± 0.017	16 (1)	...	...	$+0.000 \pm 0.018$	23 (0)	$+0.026 \pm 0.040$	23 (0)
Heske & Wendker (1984)	$+0.010 \pm 0.069$	9 (0)	...	...	-0.017 ± 0.040	9 (0)	-0.005 ± 0.040	8 (1)
Perry et al. (1990)	$+0.017 \pm 0.036$	24 (4)	...	...	$+0.013 \pm 0.015$	26 (1)	-0.009 ± 0.035	26 (1)
Sung et al. (1998)[b]	-0.016 ± 0.021	1157(148)	$+0.027 \pm 0.023$	1227(74)	$+0.012 \pm 0.018$	1114(173)	$+0.033 \pm 0.065$	998(122)
Piatti et al. (1998)	$+0.059 \pm 0.056$	58 (9)	$+0.078 \pm 0.064$	61 (6)	...	...	...	...
Baume et al. (1999)[b]	$+0.010 \pm 0.048$	466(102)	$+0.056 \pm 0.050$	493(50)	$+0.000 \pm 0.055$	496(62)	$+0.018 \pm 0.055$	271(60)

Notes.
[a] The number of stars in parenthesis is excluded in the comparison.
[b] Comparison made for $V < 16$ for $U-B$, and $V < 17$ for V, $V-I$, and $B-V$.

stars are marked by different symbols. The intrinsic and reddened MS relations (using the adopted reddening law for the $(B-V, V-I)$ diagram) are also drawn in the figures.

The $(U-B, B-V)$ diagram is the basic diagram for estimating the reddening to early-type stars. The $E(B-V)$ reddening of early-type stars in NGC 6231 is between 0.45 and 0.60 mag, but some stars have somewhat larger $E(B-V)$. The mean value of $E(B-V)$ is 0.47 mag, which is the same as the value obtained by SBL98. The low-mass PMS stars with X-ray and/or Hα emission seem to have nearly the same reddening as the massive early-type stars. But most of the normal late-type stars are slightly less reddened, and are presumably foreground field stars in the Sagittarius arm. Unlike the low-mass PMS stars in NGC 2264 (Sung et al. 1997), only a few stars show ultraviolet (UV) excesses. This means that the accretion activity of PMS stars in NGC 6231 has nearly stopped. We determined the reddening $E(B-V)$ of all early-type stars (we assumed the standard color excess ratio of 0.72 between $B-V$ and $U-B$), and calculated the spatial variation of reddening as shown in Figure 4. The dots in the figure represent the early-type stars used in the reddening determination. As already noted in SBL98, the reddening is very high in the south, relatively low in the north, and shows a local minimum near the center.

The $(B-V, V-I)$ diagram is shown in the middle panel of Figure 3. The reddened MS relation does not pass through the mean distribution of early-type stars. This is because the direction of the reddening vector in the diagram is affected by the reddening law and the adopted reddening law does not fit the early-type stars in the cluster center (see Section 3.2 for details).

The (Hα, $V-I$) diagram is presented for $V \leqslant 18$ mag in the lower panel of Figure 3. The low-mass PMS stars with Hα emission can be selected from the diagram (Sung et al. 1997). As already noticed in SBL98, there are not many Hα emission PMS stars in NGC 6231. Most X-ray emission stars do not show excess emission in Hα. We designated stars above the border line (Park & Sung 2002) as Hα emission stars. In addition, the Hα emission stars selected in SBL98 or from other studies are also designated as Hα emission stars. A total of 31 Hα emission stars and 34 Hα emission candidates were selected. Among them 18 stars are also X-ray emission stars with membership "+" or "−." The star ID 357 (=HD 326324 = Hen 3-1269) does not show any appreciable emission in our Hα photometry, but the star was classified as an Hα emission star by Henize (1976). The stars ID 294 (=Wray 15-1546; Wray 1966) and ID 6017 (=Hen 3-1281) show strong Hα emission from our Hα photometry. ID 2132 (=SBL 125) and ID 4359 (=SBL 667 = Se 166) are two massive Hα emission stars near the MS band within the cluster radius.

3.2. Reddening Law

The interstellar reddening law is one of the fundamental parameters used in determining the distance to astronomical objects, and is known to be different from sight line to sight line in the Galaxy (Fitzpatrick & Massa 2009). They confessed that there is no universal near-infrared (near-IR) extinction law. We derived similar relations between R_V and color excess ratio using their Equation (5) (the effective wavelength of *Spitzer*/IRAC (Fazio et al. 2004) bands from IRAC Instrument Handbook[7]) and power α from their Table 4. The results are

$$R_V = 1.147\frac{E(V-[3.6])}{E(B-V)} - 0.361, r = 0.998, \quad (1)$$

$$R_V = 1.098\frac{E(V-[4.5])}{E(B-V)} - 0.248, r = 0.999, \quad (2)$$

$$R_V = 1.065\frac{E(V-[5.8])}{E(B-V)} - 0.168, r = 1.000, \quad (3)$$

$$R_V = 1.038\frac{E(V-[8.0])}{E(B-V)} - 0.101, r = 1.000. \quad (4)$$

We also derived similar relations for the near-IR 2MASS bands, but the data points showed a large scatter. We decided to use the relations presented in Guetter & Vrba (1989) for near-IR JHK_s bands.

SBL98 obtained a slightly higher value of R_V for the stars in NGC 6231 ($R_V = 3.3$) using the color excess in $V-I$. In this study we try to determine the reddening law from the optical I band to the mid-infrared (mid-IR) *Spitzer*/IRAC bands. First one of the authors (M.S.B.) calculated the synthetic colors of early-type stars in the near-IR 2MASS bands as well as in the mid-IR *Spitzer*/IRAC bands. In addition, we downloaded the *Spitzer*/IRAC images from the *Spitzer* archive,[8] and measured the magnitudes of O- and B-type stars in the same way as in Sung et al. (2009). NGC 6231 was observed as a part of the GLIMPSE (Galactic Legacy

[7] http://irsa.ipac.caltech.edu/data/SPITZER/docs/iracinstrumenthandbook/
[8] http://irsa.ipac.caltech.edu/applications/Spitzer/SHA

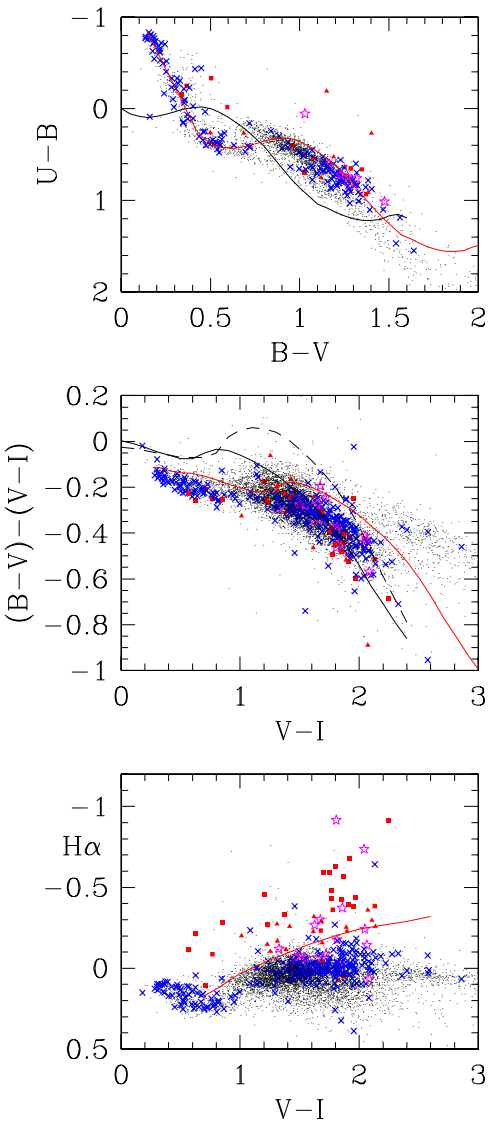

Figure 3. Color–color diagrams of NGC 6231. Top panel: the $U-B$ vs. $B-V$ diagram for $V \leqslant 16.5$ mag. Middle panel: the $B-V$ vs. $V-I$ diagram for $V \leqslant 18$ mag. Bottom panel: the Hα index vs. $V-I$ diagram for $V \leqslant 18$ mag. Thin and thick solid lines in the upper two panels represent the intrinsic and reddened ($E(B-V) = 0.47$ mag) MS relations, respectively. The dashed line in the middle panel presents the intrinsic relation of giant stars, while the thin solid line in the lower panel represents the Hα index vs. $V-I$ relation for normal MS stars (Park & Sung 2002), but shifted by 0.2 mag in $V-I$. Crosses, asterisks, squares, and triangles denote, respectively, X-ray emission stars, X-ray emission stars with Hα emission, Hα emission stars, and Hα emission candidates.

(A color version of this figure is available in the online journal.)

Infrared Mid-Plane Survey Extraordinaire) survey, but only part of the cluster was observed. Our photometric data are compared with those in the GLIMPSE Point Source Archive (http://irsa.ipac.caltech.edu/data/SPITZER/GLIMPSE/), and the results are $\Delta[3.6] = +0.003 \pm 0.132$ ($n = 14$), $\Delta[4.5] = -0.003 \pm 0.071$ ($n = 21$), $\Delta[5.8] = +0.038 \pm 0.115$ ($n = 14$), and $\Delta[8.0] = +0.032 \pm 0.063$ ($n = 21$).

The color excess relations between $B-V$ and other colors are presented in Figure 5. Although many early-type stars with $E(B-V) = 0.4$–0.6 show a large scatter, if we use the stars with $E(B-V) \geqslant 0.6$, the color excess ratios are very close to the normal value. Using the relations between R_V and color excess ratios, the total-to-selective extinction ratio R_V of the stars in NGC 6231 is 3.22 ± 0.04 from eight optical to mid-IR colors.

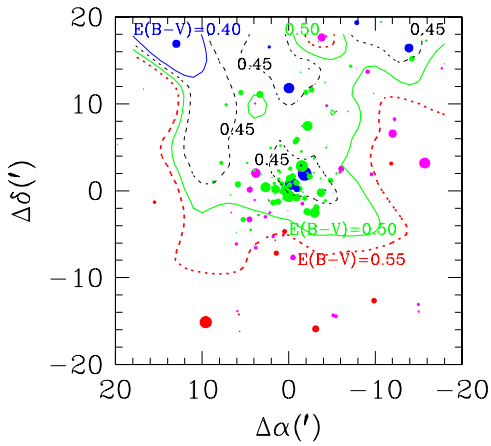

Figure 4. Smoothed reddening map of NGC 6231. The lines represent the iso-reddening contours smoothed with the scale length of 1′. The line type and thickness represent different amount of reddening $E(B-V)$ as shown in the figure. The dot represents the early-type stars used in reddening determination.

(A color version of this figure is available in the online journal.)

This value implies that the reddening law toward NGC 6231 is very close to normal. We adopt $R_V = 3.2$ for NGC 6231. This value is the same as the total-to-selective extinction ratio toward the intermediate-age open cluster M11 (Sung et al. 1999).

In addition, the stars near the cluster center show somewhat larger color excess ratios, as seen in Figure 6. The abscissa is the distance from the center of the polarization angle (Feinstein et al. 2003). But when the abscissa is distance from the cluster center, the result does not differ very much. The stars at larger distance from the cluster center ($r_{\rm pol} > 14'$) show very normal ratios, but stars in the inner region show large values and a large scatter. The R_V of the inner region from four optical and near-IR bands is 3.43 ± 0.04. SBL98 proposed that the deficit of low-mass PMS stars with Hα emission and the hole seen in reddening map are due to the stellar wind from massive stars, WR stars or past supernova explosion(s). This higher value of the color excess ratios in the cluster center may also be related to these effects.

The extra extinction due to the slightly higher value of the color excess ratios of the stars in the cluster center is about 0.04–0.05 mag in V and 0.02 mag in $V-I$, if we assume the foreground reddening toward the Sagittarius arm to be $E(B-V)_{fg} = 0.2$–0.25 mag (Sung et al. 2000). This extra extinction may slightly influence the distribution of stars in the middle panel of Figure 3 and the upper panel of Figure 7.

3.3. Color–Magnitude Diagrams and Distance

The color–magnitude diagrams (CMDs) of NGC 6231 are presented in Figure 7. From the CMDs at the top left we can easily recognize the well-developed sequence of early-type MS/post-MS members in the left of each CMD. The zero-age main sequence (ZAMS) with mean reddening and adopted distance is overplotted. In addition, a few PMS evolution tracks of Siess et al. (2000) and the 1 $M_\odot$ evolution model of Baraffe et al. (1998) are superimposed. The empirical color–temperature relations for low-mass stars of Bessell (1995) and synthetic color–temperature relations of Bessell et al. (1998) were employed in the transformation of physical parameters to observational colors.

Most of the O- and early B-type stars in NGC 6231 are X-ray emitters. In addition, many faint X-ray emission stars are about 3 mag brighter than the adopted ZAMS line, and have

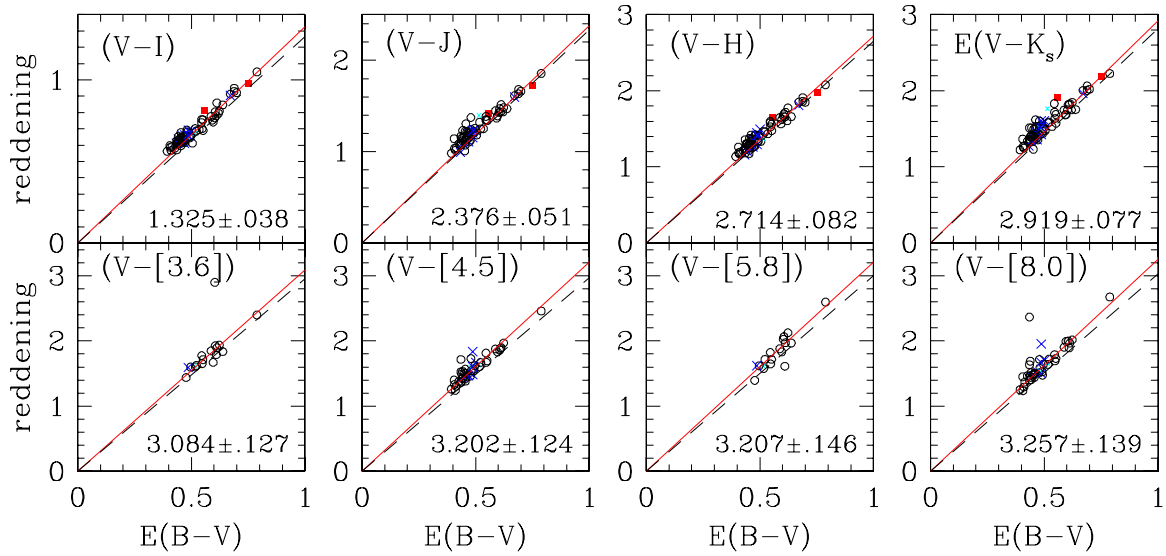

Figure 5. Reddening law of NGC 6231 from the optical to mid-IR. The reddening for a given color with respect to $E(B-V)$ is shown. The optical and mid-IR data are from this study, while near-IR data are from 2MASS. The dashed and solid lines represent the normal reddening law ($R_V = 3.1$) and the reddening law for NGC 6231, respectively.

(A color version of this figure is available in the online journal.)

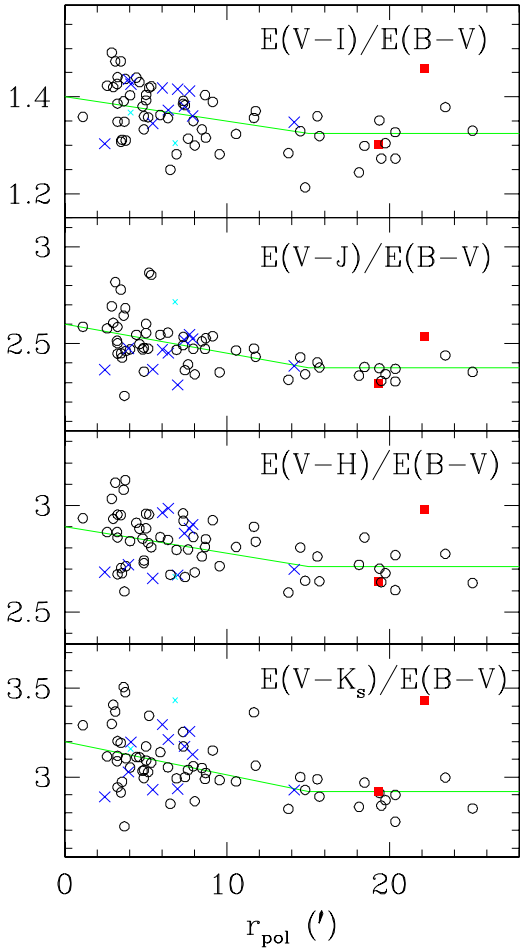

Figure 6. Radial variation of color excess ratios. The radial distance in minutes of arc is measured from the center of polarization angle (Feinstein et al. 2003). Squares and crosses represent stars with Hα and X-ray emission, respectively. The early-type stars in the field region show a nearly normal ratio, but those in the cluster show a large scatter.

(A color version of this figure is available in the online journal.)

the typical brightness of PMS stars in young open clusters. There are not as many X-ray emission stars at $V-I \approx 1.0$, but stars in the lower MS and transition zone are mostly X-ray emission stars. The stars at $V-I \approx 1.0$ are field stars at a similar distance to NGC 6231. They are relatively old disk stars in the Sagittarius arm, and therefore they are mostly inactive in X-rays. In addition, the small number of X-ray emission stars implies that the PMS stars evolve quickly at this stage.

There are five early-type Hα emission stars with $V-I < 1.0$. Two of them are within the cluster radius (see Section 3.4 for the radius of NGC 6231), the brighter three (ID 294 = Wray 15-1546; ID 357 = HD 326324 = Hen 3-1269; ID 6017 = ALS 3833 = Hen 3-1281) are outside the radius of NGC 6231. There are two X-ray emission stars at $V-I \approx 0.6$ and $V \approx 10.5$ (ID 1499 = SBL 19 = HD 326343, B1V; ID 4840 = CD-41 11062B). These two stars are more reddened ($E(B-V) = 0.67$ and 0.71, respectively) than the other early-type stars. ID 4840 is the fainter component of CD-41 11062, and is an optical double with ID 4842.

The distance modulus of NGC 6231 can be determined from the distribution of the distance moduli of individual early-type stars after correcting for interstellar reddening. The extra extinction mentioned above does not seriously affect the estimate of distance to NGC 6231 because the distance modulus of individual early-type stars is estimated using the ZAMS relation in the $(V, B-V)$ diagram. The distribution shows a peak at $V_0 - M_V = 10.6$–11.0 mag, and only a few stars with a larger value. We adopt the distance to NGC 6231 as $V_0 - M_V = 11.0$ mag. This value is in excellent agreement with the value obtained by Sana et al. (2005). Although there is a slight difference in the adopted reddening law, this value is identical to the value obtained by SBL98 and adopted by Sana et al. (2006). The adopted distance modulus and mean reddening were applied in Figure 7.

We also checked the completeness of our photometry in the ΔV ($\equiv V - V_{\rm bright}$) versus distance from the nearest bright star. If the brightness of a star is brighter than or comparable to the local brightness around a bright star, the brightness of the star can be measured. But if the brightness of a star is fainter than or

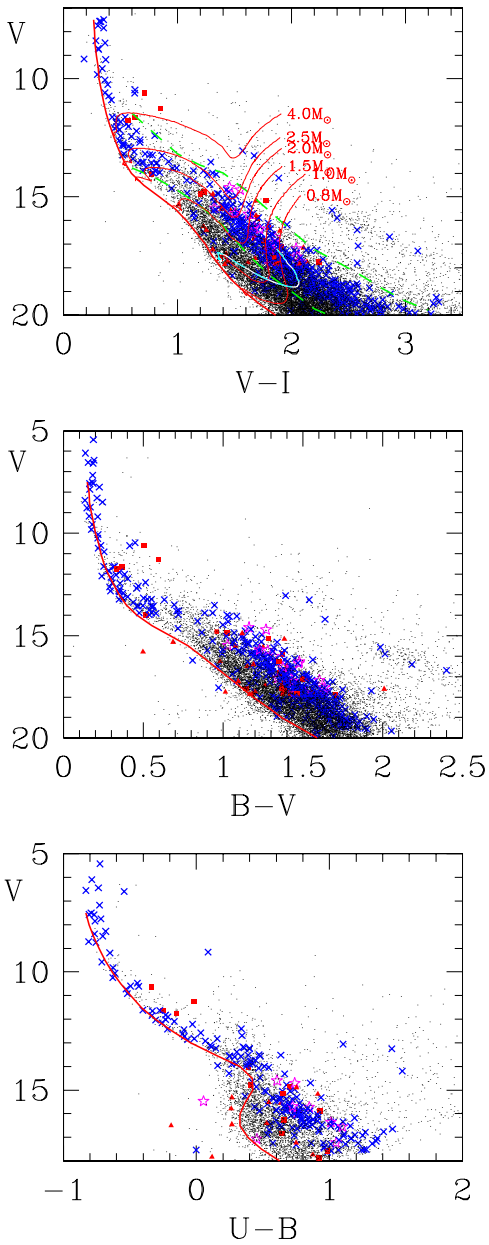

Figure 7. Color–magnitude diagrams. Top panel: the $V-I$ vs. V diagram. The thick solid line represents the reddened ZAMS relation at the NGC 6231 distance. The thin solid lines are the PMS evolution tracks of Siess et al. (2000), while the thin dashed line overlaid on the thick white solid line is the 1 $M_{\odot}$ PMS evolution track of Baraffe et al. (1998). The dashed lines in the redder part of the reddened ZAMS line represent the upper and lower limit of the adopted locus of PMS stars in NGC 6231. Middle panel: the $B-V$ vs. V diagram. Bottom panel: the $U-B$ vs. V diagram. The other symbols are the same as Figure 3.

(A color version of this figure is available in the online journal.)

comparable to the local fluctuation of surface brightness around a bright star, the brightness of the star cannot be measured. And therefore the existence or nonexistence of a faint star in the photometric catalog is a function of the distance from a bright star as well as the difference in brightness between two stars. The tracing of the avoidance zone makes it possible to estimate the area of the incomplete zone due to the presence of bright stars. And thus the ratio of the total area and the area of the incomplete zone could represent the completeness of the photometry. As the seeing is one of the important factors affecting the completeness of photometry, the completeness from this method is for the case of bad seeing of 2000 June 22. The completeness of $V = 19$ mag stars at the cluster center ($r \leqslant 2'$) is about 60%, but is higher than 80% at $r > 2'$. Although the limiting magnitude of our photometry is about $V = 20.5$ mag, the magnitude of over 80% completeness, is about $V = 19$ mag, except for the cluster center ($r \leqslant 2'$). The dashed lines in the V versus $V-I$ diagram are the apparent loci of PMS stars (X-ray emission stars and Hα emission stars) of NGC 6231. From the completeness test results, our photometry is about 80% complete for PMS stars with mass $\gtrsim 0.8\ M_{\odot}$, except for the cluster center ($r \leqslant 2'$).

There is a relatively well-defined sequence of foreground stars in the CMDs. They are about 5.5 mag brighter than the adopted ZAMS of NGC 6231. Several X-ray emission stars can be found in the sequence. The distance to the foreground objects is about 130 pc. As NGC 6231 is located at the southeastern edge of the Upper Centaurus-Lupus group of the Sco-Cen OB association, the stars are likely members of the Upper Centaurus-Lupus moving group.

3.4. Surface Density Profiles and the Radius of NGC 6231

NGC 6231 is the core cluster of the Sco OB1 association, and therefore the radius of the cluster is not easy to determine because many members of the Sco OB1 association, as well as field stars in the Sagittarius arm, are seen in the same sight line. In particular, the photometric characteristics of Sco OB1 association members are very similar to those of the cluster members.

To determine the radius of NGC 6231, we assigned the membership of each star. Stars with $V \leqslant 13$ mag and $U-B \leqslant 0.0$ mag were classified as massive MS members of NGC 6231. And stars in the PMS locus (the upper panel of Figure 7) were classified as PMS members if X-ray emission and/or Hα emission was detected, or as PMS candidates if no membership information was available. Next we determined the center of NGC 6231 from the geometric center of stars with a certain brightness limit. Different brightness limits gave a slightly different value, but the difference was not large. We calculated the geometrical center of the massive MS members with masses greater than about 5 $M_{\odot}$ ($V \approx 11$ mag) and adopted this as the center of NGC 6231. The adopted center of NGC 6231 is $\alpha_{\rm J2000} = 16^{\rm h}54^{\rm m}11^{\rm s}.7$, $\delta_{\rm J2000} = -41^{\circ}50'20''$, which is approximately equidistance from HD 152248 (O7.5III+O7III(f), Sana et al. 2001); HD 152249 (O9Ib(f), Sana et al. 2008) and HD 152270 (WC7+O6V, Hill et al. 2000).

We calculated the surface density profiles for four member groups: massive MS/post-MS members ($V \leqslant 10$, equivalently $m \gtrsim 10\ M_{\odot}$), intermediate-mass MS stars ($V = 10$–13, equivalently $m = 10$–2.5 $M_{\odot}$), bright PMS stars ($V \leqslant 15$ in PMS locus), and faint PMS stars ($V = 15$–18 in PMS locus), and these are shown in Figure 8. In the calculation of surface density, we used an annulus width of $1'$ for three faint groups, but a $2'$ width was used for the bright massive group because of the small number of massive stars. In addition, we also calculated the surface density of presumably non-member stars (bright field stars—stars brighter and redder than the PMS locus; faint field stars—stars fainter and bluer than the PMS locus). The error in the surface density is assumed to follow Poisson statistics, i.e., $\epsilon = \sqrt{N}/S$ (where N and S are the number of stars and the area of the annulus, respectively). As expected, the surface density profiles of field stars did not show any radial variation. The results are summarized in Table 4.

The fifth column of Table 4 represents the contrast of surface densities between cluster and field. The contrast is very high for

Table 4
Summary of Surface Density Analysis

Group	V Range	$\rho_{\rm cnt}$[a]	$\rho_{\rm fd}$[a]	$(\rho_{\rm cnt}-\rho_{\rm fd})/\rho_{\rm fd}$	$N_{\rm star}$
Massive MS/post-MS	$\leqslant$10	1.11	1.34×10^{-2}	82.1	45
MS stars	10–13	2.86	5.00×10^{-2}	56.2	145
Bright PMS	$\leqslant$15	2.23	3.94×10^{-1}	4.7	567
Faint PMS	15–18	4.46	1.41	3.2	1817
Bright non-member	Above PMS locus	...	1.68	...	1901
Faint non-member	Below PMS locus	...	1.74	...	1979

EFF Profile Fitting Parameters

	μ_0 (pc^{-2})	a (pc)	γ	$r_{\rm c}$ (pc)	n_0 (pc^{-3})	$N_{\rm tot}$
Massive MS/post-MS	6.80 ± 0.38	1.63 ± 0.04	5.45 ± 0.07	0.88 ± 0.02	0.048 ± 0.005	32.88
MS stars	10.18 ± 1.73	1.39 ± 0.18	2.97 ± 0.22	1.07 ± 0.14	0.090 ± 0.042	127.15
Bright PMS	10.16 ± 1.46	8.96 ± 1.21	42.34 ± 0.52	1.63 ± 0.22	1.791 ± 0.094	126.93
Faint PMS	10.21 ± 1.63	7.48 ± 3.42	17.25 ± 1.65	2.16 ± 0.99	6.494 ± 0.227	235.32

Note. [a] Surface density at center and field region ($r>10'$), respectively. Unit: #/□′.

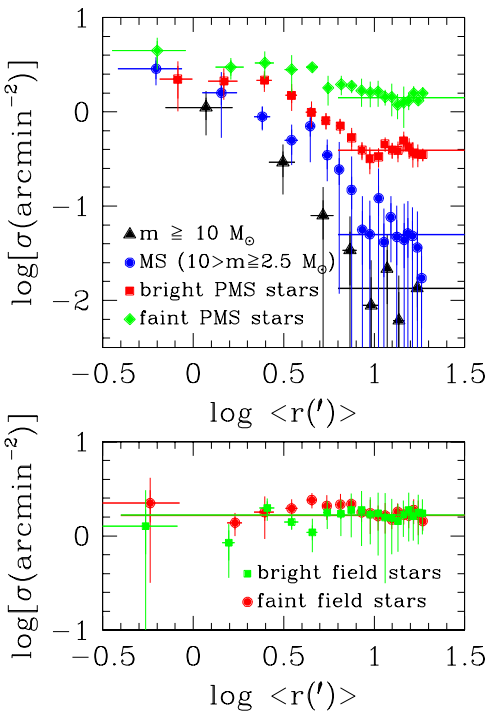

Figure 8. Surface density profiles. Upper: surface density profiles of MS stars and stars in the PMS locus of NGC 6231. The horizontal bars represent the average surface density of field region ($r>10'$). Lower: surface density profiles of the field stars above and below the PMS locus of NGC 6231. The widths of the annuli are 1′ for all groups except the most massive group ($\Delta r=2'$).

(A color version of this figure is available in the online journal.)

MS and evolved massive stars, but those of PMS stars are very low. The surface density of MS/post-MS stars shows a large fluctuation at $r\gtrsim10'$ due to the small number of early-type stars in the field. Although there are large differences in surface density variation among member groups, the surface density of each group reaches the level of the surface density of the field region at $r\approx10'$ regardless of the stellar mass. From the radial variation of surface density profiles, the radius of NGC 6231 was adopted to be 10′.

We also attempted to fit the cluster surface density profiles to a King empirical density profile of a spherical system (King 1962), as shown in the left panel of Figure 9. As expected, the tidal radii of all groups were very similar to each other, and between 10′ and 20′. But the core radius varied systematically from 1.′5 to 5.′5. As King profiles are strictly speaking not appropriate for open clusters, we also fitted the cluster surface density using Elson et al.'s (1987) profiles (EFF profiles). The best-fit EFF profile parameters are presented in Table 4. Using the best-fit values, we computed the core radius of the EFF profile, i.e., the radius at which the surface density drops to half its center value. As for the King profile, we observed a systematic increase from 1.′9 to 4.′7 (corresponding to 0.9–2.2 pc given $V_0-M_V=11.0$) for populations with decreasing masses. Both King and EFF profile fittings imply a mass segregation within NGC 6231—massive stars are more concentrated in the cluster center, while faint PMS stars are more widely distributed. We will come back to this aspect in Section 4.5.

4. THE INITIAL MASS FUNCTION AND THE AGE OF NGC 6231

4.1. Adopted Calibrations and Stellar Evolution Models

In SBL98 and our studies on other young open clusters, we used the spectral-type–temperature scale of Crowther (1997) for O-type stars. Advances in astronomical instruments, observing techniques, and non-LTE model atmospheres have made an appreciable change in the temperature scale of massive O-type stars. In this study, the spectral-type–temperature scale of O-type stars of Martins et al. (2005) is adopted. Their calibration gives somewhat lower temperatures, and hence smaller bolometric corrections for O-type stars than that of Crowther (1997). For intermediate- and low-mass stars no significant change in the temperature scale was made, and therefore the same calibrations were used as in Hur et al. (2012).

In the 2000s, stellar rotation was introduced in the evolutionary models of massive stars (Meynet & Maeder 2000). But in most studies the stellar evolution models by Schaller et al. (1992) were used because new models with stellar rotation were limited to only a few high masses. Recently, new stellar evolution models with rotation covering a wide mass range were published (Ekström et al. 2012; Brott et al. 2011). The stellar evolution models by Brott et al. (2011) are limited for the stars with masses 5–60 $M_\odot$. This mass range is useful for NGC 6231, but our long-term project for investigating the shape of the IMF of young massive clusters (e.g., see Hur et al. 2012; Lim et al. 2012) requires a much wider range of stellar masses. In this study, we

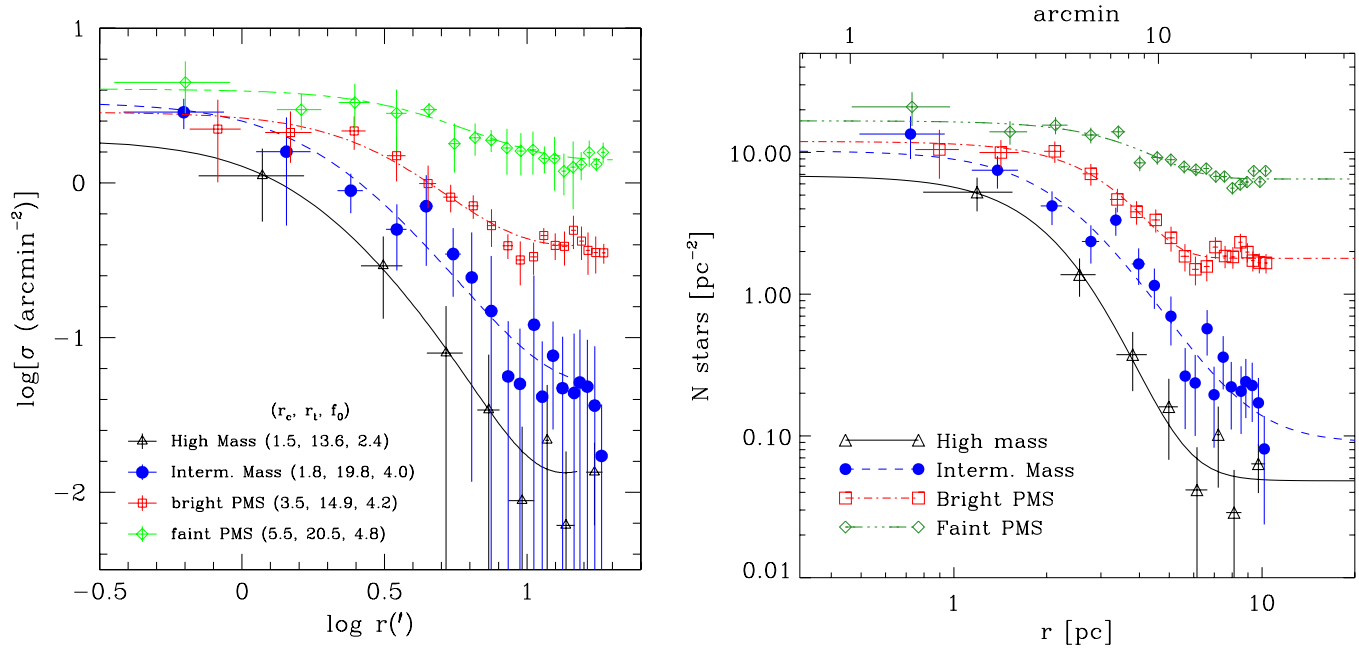

Figure 9. Surface density profile fittings. Left: King profile fits. Right: EFF profile (Elson et al. 1987) fits. Note that the two figures use different units.
(A color version of this figure is available in the online journal.)

will mainly use the stellar evolution models by Ekström et al. (2012) that include a moderate initial rotation ($v_{\rm eq} = 0.4 v_{\rm crit}$, thus ≈220 km s^{-1} for massive MS stars). Although the final ZAMS temperatures and luminosities of a 1 $M_\odot$ star are very similar to each other, the detailed evolutionary tracks of Baraffe et al. (1998) and Siess et al. (2000) differ from each other as shown in Figure 7. As the models by Siess et al. (2000) cover a relatively large mass range, we will use the PMS evolution models by Siess et al. (2000) for the age and mass estimate of low-mass PMS stars.

4.2. Hertzsprung–Russell Diagram and Age of NGC 6231

The age of an open cluster can be determined by comparing the observations with theoretical stellar evolution models. The HRD is the basic diagram to diagnose a stellar system. To construct the HRD of NGC 6231, we should correct the interstellar reddening of individual stars. For early-type stars the reddening is estimated from the color–color diagram and applied individually. But for low-mass PMS stars, as there is no direct way to estimate the reddening from photometric data alone, the reddening of these stars are estimated from the reddening map presented in Figure 4. Using the adopted calibrations, we transformed the reddening-corrected colors to physical parameters, such as effective temperature and bolometric magnitude. For massive O- and early B-type stars, the spectral type is the most important indicator of the effective temperature and hence bolometric correction as well.

The HRD of NGC 6231 is presented in Figure 10. The theoretical ZAMS and two isochrones of ages 4 Myr and 7 Myr are superimposed. These isochrones were derived by interpolating the theoretical stellar evolution tracks of Ekström et al. (2012) and the PMS evolution tracks of Siess et al. (2000). The age of massive stars in NGC 6231 is between 4 Myr and 7 Myr. This is somewhat larger than the age obtained by SBL98 (2.5–4 Myr). Although there was a change in the stellar evolution models used in the age estimate, the main cause of the big difference in age is the change in the adopted calibrations,

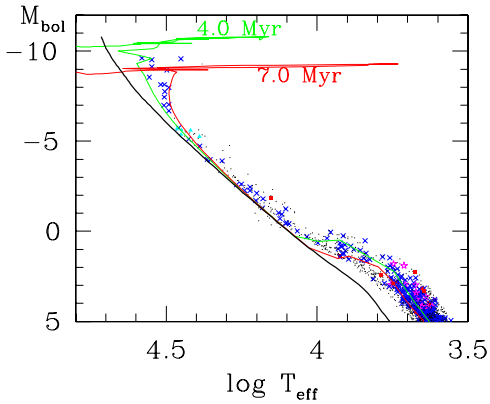

Figure 10. Hertzsprung–Russell diagram of NGC 6231. Triangles represent variables. The other symbols are the same as Figure 3.
(A color version of this figure is available in the online journal.)

especially for massive O-type stars. For another young open cluster Westerlund 1, the new and old stellar evolution models from the Geneva group (Ekström et al. 2012; Schaller et al. 1992) do not give any significant difference in age (Lim et al. 2012). However, the stellar evolution models by Brott et al. (2011) give a slightly younger age (3–4 Myr) for NGC 6231 (see Section 5.2 for details).

The situation for PMS stars is the opposite—the age of low-mass PMS stars are younger than presented in SBL98. Many PMS members and candidates are slightly redder than the 4 Myr isochrone. The age distribution of low-mass PMS stars is shown in Figure 11. The histograms show the age distribution of all PMS stars in the PMS locus and are corrected for the contribution of interlopers (Sco OB1 association members and field stars), respectively. As the PMS evolution models do not give a consistent age for the whole mass range (Sung et al. 2004; see also Sung et al. 1997), the distribution is derived only for those PMS stars with masses between 0.8 and 1.0 $M_\odot$. The age of low-mass PMS stars is between 1 Myr and 7 Myr (Sana et al.

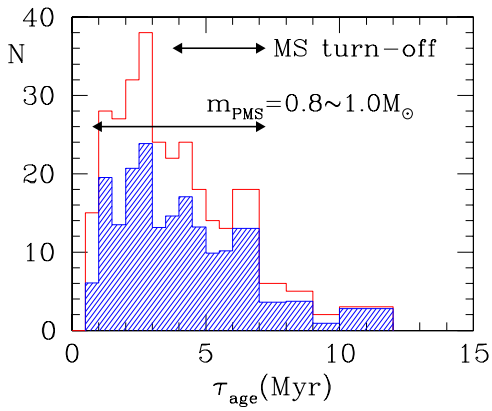

Figure 11. Age distribution of stars in NGC 6231. White and hatched histograms represent, respectively, the age distribution of all the low-mass PMS stars within the cluster radius, and those that have been statistically subtracted for the contribution of field stars.

(A color version of this figure is available in the online journal.)

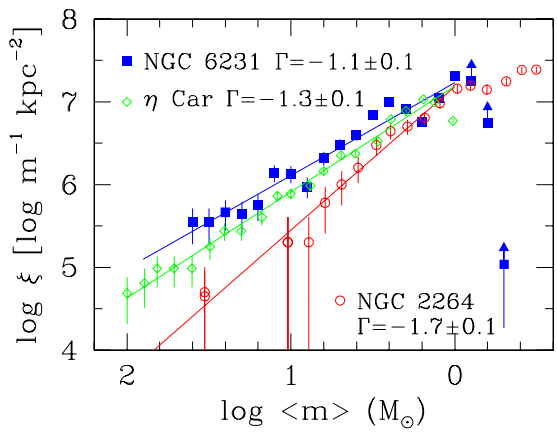

Figure 12. IMF of NGC 6231. Filled squares are the IMF of NGC 6231, while open circles and open diamonds are that of NGC 2264 (Sung & Bessell 2010) and the η Carina Nebula (Hur et al. 2012). The solid lines represent the least-square fit to the IMFs. The slope of the IMF (Γ) is calculated for the stars with $\log m > 0.2$.

(A color version of this figure is available in the online journal.)

(2007) also found a similar spread of age of low-mass PMS stars), and therefore the age spread is about 6 Myr, which is the typical spread from CMD analysis (Sung & Bessell 2010).

4.3. The Initial Mass Function

The mass of an individual star is estimated from the HRD. For massive stars it is not easy, because a small difference in age gives a very different position in the HRD, and it is therefore impossible to use a single isochrone or mass–luminosity relation. In addition, the complex evolutionary tracks of massive stars make this matter even more difficult. We tried another way to estimate the mass of massive stars—the mean initial mass of stars at a given point in the HRD is calculated from a Monte Carlo simulation of a stellar system. A few million stars with masses larger than 20 $M_\odot$ were generated for about 500 Myr at a constant rate. The stellar masses were generated according to an IMF with Salpeter type slope ($\Gamma = -1.3$). In the model calculation, stars were evolved according to the recent stellar evolution models of Ekström et al. (2012). From the model, we calculated the mean mass and age of stars within the specified photometric box in the HRD. From this database we calculated the mass and age of massive evolved stars.

The mass of intermediate-mass MS stars was estimated using the mass–luminosity relation of stellar evolution models. The mass of PMS stars was estimated by interpolating the PMS evolution models of Siess et al. (2000). And then the number of stars in a logarithmic mass interval of $\Delta \log m = 0.2$ was calculated. The number of stars in the field region was also calculated in the same way. After subtracting the contribution of field stars, the cluster mass function was then obtained by dividing the projected area and mass interval. To minimize the effect of binning, we also calculated the mass function by shifting the mass bin by $\log m = 0.1$. Actually we only estimated the initial mass of individual stars, not the current mass of the star. Therefore the mass function is the same as the IMF except for the most massive bin for the clusters with age $\geqslant 3.5$ Myr. For NGC 6231, the mass function obtained here is the IMF of NGC 6231 for $m \lesssim 45\,M_\odot$.

The IMF of NGC 6231 is presented in Figure 12. The IMFs of NGC 2264 (Sung & Bessell 2010) and the η Carina Nebula Hur et al. (2012) are also presented. The slope of the IMF of NGC 6231 is slightly shallower than that of the η Carina Nebula, but the difference is marginal because the shallow slope is partly caused by the dearth of stars at $\log m \approx 0.2$. But the difference between NGC 6231 and NGC 2264 is evident. The slope of NGC 2264 is very steep. Although the surface density at $\log m \approx 0$ is very similar, the surface density at $\log m \approx 1$ of NGC 6231 is about 10 times higher than that of NGC 2264. Recently, Damiani et al. (2009) obtained a slightly steep IMF ($\Gamma = -1.3$ to -1.5) for NGC 6231. Such a difference in the IMF slope may be caused by the difference in the adopted distance, the amount of reddening correction, and/or the adopted stellar/PMS evolution models.

4.4. The Total Mass of NGC 6231

The total mass of a cluster is an important parameter. Recently, Weidner et al. (2010) studied the relation between the most massive star and its parental cluster mass. They classified clusters into three categories according to their total cluster mass: lowest mass clusters ($M_{cl} \leqslant 10^2 M_\odot$), moderate mass clusters ($10^2\,M_\odot < M_{cl} \leqslant 10^3 M_\odot$), and rich clusters ($M_{cl} > 10^3\,M_\odot$). And they found a plateau of a constant maximal star mass ($m_{max} \approx 25\,M_\odot$) for clusters with masses between $10^3\,M_\odot$ and $4 \times 10^3\,M_\odot$.

We calculated the total mass of NGC 6231 by simulating model clusters using a Monte Carlo method. For the model clusters we assumed the IMF of NGC 6231 in four cases for the low-mass regime: (1) the IMF of NGC 6231 and that of NGC 2264 (Sung & Bessell 2010) were adjusted between $\log m = 0.6$–0.4, and we used the adjusted IMF of NGC 2264 for $\log m < 0.4$; (2) the IMF of NGC 6231 and that of NGC 2264 were adjusted between $\log m = 0.2$–0.0, and we used the adjusted IMF of NGC 2264 for $\log m < 0.0$; (3) the IMF of NGC 2264 was used for $\log m < 0.0$ without any adjustment; and (4) the IMF of Kroupa (2002). For the massive part of the first three cases, we simply extrapolated the IMF of NGC 6231 up to $\log m = 2.0$. We assumed the upper mass limit of stellar mass as 100 $M_\odot$, and an age spread of about 3 Myr (age: 4–7 Myr) for the massive stars ($m \geqslant 30\,M_\odot$) as obtained in Section 4.2. A total of 100,000 stars were generated, and a scaling factor was calculated to reproduce the number of stars with masses between $\log m = 0.4$–1.0. The total masses estimated were $3.0 \times 10^3\,M_\odot$, $2.2 \times 10^3\,M_\odot$, $2.1 \times 10^3\,M_\odot$, and $3.3 \times 10^3\,M_\odot$, respectively. And therefore the total mass of NGC 6231 is $2.6\,(\pm 0.6) \times 10^3\,M_\odot$. This value is slightly smaller

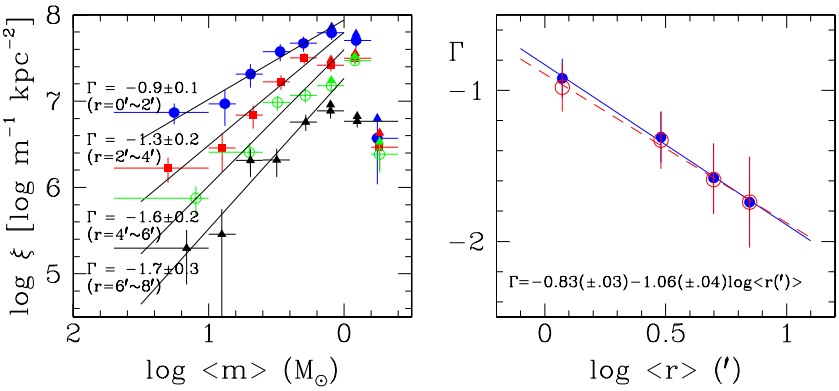

Figure 13. Radial variation of the IMF. Left: the IMF at different radii. Right: the radial variation of the slope of the IMF. The large dots, the solid line, and the slope gamma represent the radial variation for the case of no correction for the data incompleteness, while open circles and a dashed line are corrected for the data incompleteness. The slope of the IMF varies systematically from cluster center to the outer region. The IMF at the outermost region is not shown because of its large uncertainty due to the small number of cluster stars.

(A color version of this figure is available in the online journal.)

than the total mass of NGC 6231 ($4595^{-2312}_{+4676}\ M_\odot$) estimated by Weidner et al. (2010). Such a large discrepancy in the total mass may be related to the subtraction of field contamination, especially for stars in the Sco OB1 association.

4.5. MASS SEGREGATION

Mass segregation in young open clusters is a hot issue in the dynamical evolution of star clusters. McMillan et al. (2007) proposed a plausible scenario for mass segregation as mentioned in the introduction. NGC 6231 is an important target for such a study as the cluster is little obscured, has many members, and relatively small differential reddening across the cluster. To see the extent of mass segregation in NGC 6231, we calculated the radial variation of the IMF as shown in Figure 13. The IMF for each ring (width of the ring $= 2'$) was calculated in the same way as in Section 4.3. But as the number of massive stars was very small, only one mass bin was used for the stars more massive than 10 $M_\odot$. For the outermost ring ($r = 8' \sim 10'$), the number of stars in the ring, after subtracting the field contribution, was negative in many cases, and therefore we did not try to calculate the IMF for the ring. The completeness of photometry was better than 90% even in the innermost ring for $\log m > 0.4$, so we did not correct for the effect of data incompleteness in the left panel of Figure 13. But the effect of incompleteness in $\log m < 0.4$ cannot be neglected, especially for the innermost ring where the crowding effect is most severe. In the right panel of Figure 13, we also calculated and presented the slopes of the IMF for a given ring, with and without correction for data incompleteness.

As can be seen in Figure 13, the slope of the IMF increases systematically from the center to the peripheral region. The slope of the IMF in each ring was calculated, and shows a variation with radius from the cluster center (right panel). The slope of the IMF varies systematically—it is very shallow in the center and very steep at the peripheral regions. The right panel of Figure 13 shows that the mass segregation in NGC 6231 is evident and very systematic.

Allison et al. (2009a) introduced a parameter, the mass segregation ratio $\Lambda_{\rm MSR}$, to detect and quantify the level of mass segregation in a cluster. The $\Lambda_{\rm MSR}$ compares the path length from the minimum spanning tree of a certain kind of objects and that of random samples. The merit of this method is that the $\Lambda_{\rm MSR}$ is insensitive to uncertainty in determining the center of an open cluster. Sana et al. (2010) applied this method to the young compact cluster in the η Carina Nebula, Trumpler 14, and found a signature of mass segregation for bright members ($m \gtrsim 10\ M_\odot$), and marginal mass segregation for less bright members ($K_s \lesssim 10.5$ mag). We also calculated the mass segregation ratios for member stars (MS stars and PMS stars in the PMS locus within the adopted cluster radius) and present it in Figure 14. In the calculation of $\Lambda_{\rm MSR}$, we used the same bin size ($N = 20$). The most massive two bins ($m \gtrsim 8\ M_\odot$) show a distinct mass segregation, and stars with masses between 10 and 3 $M_\odot$ are marginally mass segregated. It is worth noting that as the completeness of photometry is lower for the fainter stars, especially fainter stars in the center, the $\Lambda_{\rm MSR}$ is affected by the data incompleteness. Given the limitation, we can say that massive stars ($m \gtrsim 8\ M_\odot$) in NGC 6231 are mass segregated. Discussion on the origin of mass segregation is presented in Section 5.3.

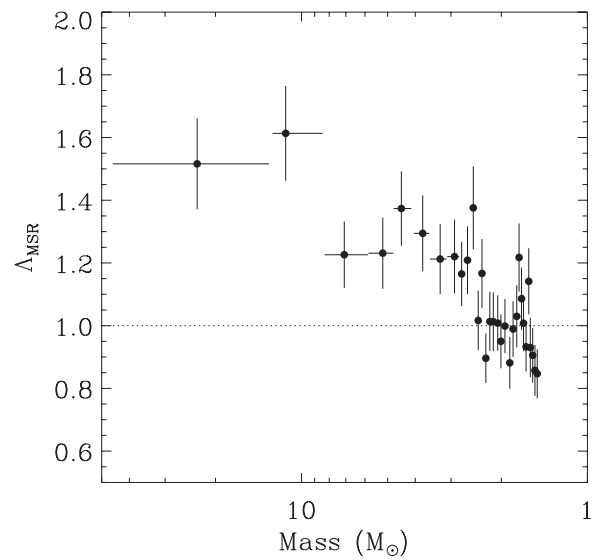

Figure 14. Relation between the mass segregation ratio ($\Lambda_{\rm MSR}$) and the stellar mass. The number of member stars in each bin is 20. The dot represents the average mass of each bin, and the horizontal bar represents the range of stellar masses for a given bin. The $\Lambda_{\rm MSR}$ of the stars with $m \gtrsim 3\ M_\odot$ shows mass segregation, while those of low-mass stars have about unity ($\Lambda_{\rm MSR} \approx 1$—no mass segregation).

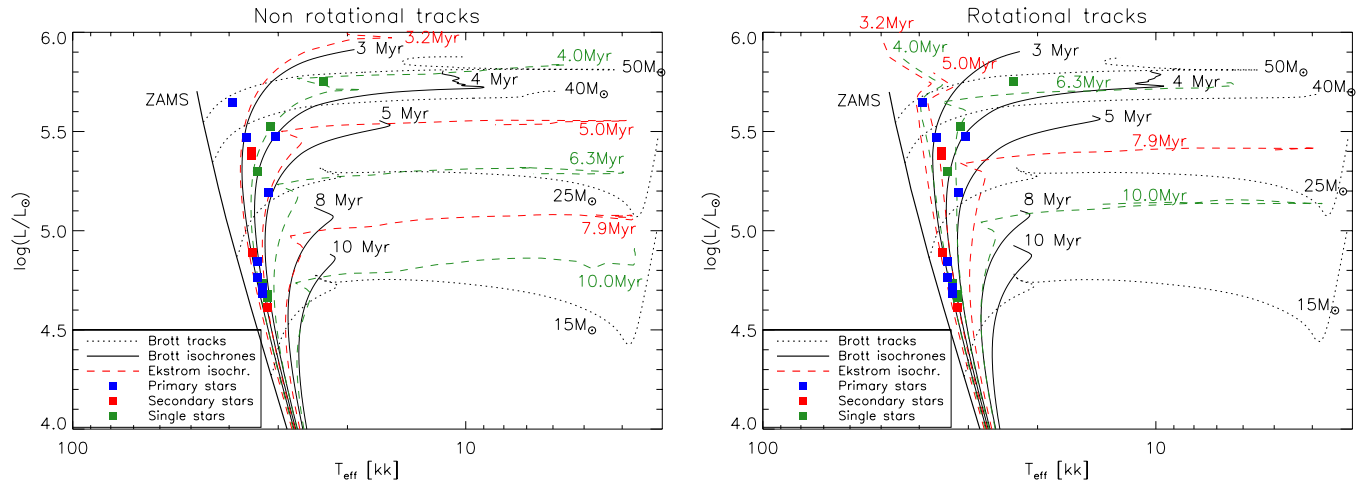

Figure 15. Upper part of the Hertzsprung–Russell diagram. Left: non-rotating models; right: rotating models.

(A color version of this figure is available in the online journal.)

5. DISCUSSION

5.1. HD 153919

The runaway O6.5Iaf star HD 153919 has been proposed to have originated from Sco OB1 (Bessell et al. 1974; Ankay et al. 2001). If the location of HD 153919 ($\mu_\alpha = 2.80 \pm 0.59$ mas yr^{-1}, $\mu_\delta = 4.71 \pm 0.32$ mas yr^{-1}; van Leeuwen 2007) before the supernova explosion is assumed to be at the center of the distribution of polarization vectors (Feinstein et al. 2003), we can check whether or not that is a reasonable assumption, on the basis of stellar evolution theory. As the angular distance between the polarization center and HD 153919 is ($\Delta\alpha = 1\overset{\circ}{.}92$, $\Delta\delta = 3\overset{\circ}{.}84$, $\rho = 4\overset{\circ}{.}29$), the proper motion of the star should have the minimum value ($\mu - \epsilon_\mu$) for the star to have crossed NGC 6231 in the past. And therefore if we take the proper motion of the star as $\mu'_\alpha = 2.21$ mas yr^{-1}, $\mu'_\delta = 4.39$ mas yr^{-1}, then the star would have been ejected from the polarization center 3.14 ± 0.01 Myr ago. As the age of massive stars in NGC 6231 is 4–7 Myr, the past supernova exploded when the age of NGC 6231 was 1–4 Myr.

The lifetime of the most massive star (120 $M_\odot$) in Ekström et al. (2012) is 3.5 Myr, and that of a 85 $M_\odot$ is 4.0 Myr. If HD 153919 originated from NGC 6231, the initial mass of the supernova progenitor would be 85 $M_\odot$, or larger. This result is consistent with the current stellar evolution models and the IMF of NGC 6231, as we could expect 2–3 stars more massive than the most massive star in the current NGC 6231. While the end product of the evolution of a star typically more massive than 25 $M_\odot$ is expected to be a black hole, a massive star may end its life as a neutron star, if it loses enough mass through wind-driven mass loss (Fryer et al. 2002) and/or binary interaction with a lower mass companion. As most massive stars are in close binary systems (Sana et al. 2008), part of the primary's mass is likely to be transferred to the companion during the MS stage or in later evolutionary stages, and finally it becomes a neutron star after a supernova explosion. Given that HD153919 is a high-mass X-ray binary, the second scenario is the more likely.

5.2. Age of Massive Stars

The current state-of-the-art stellar evolution models do include the effect of stellar rotation. It is beyond the scope of this discussion to provide a comparison between the different assumptions as well as the implementation of different physical mechanisms; however, we tested the impact of adopting the different available models on the derived properties of the high-mass stars, and more specifically on their derived age.

Figure 15 (left panel) compares the isochrones obtained from the non-rotating evolutionary models of Brott et al. and Ekström et al. The main difference resides in the position of the end of the MS in the HRD and results from different assumptions on the value of the core overshooting parameter. The age derived for the massive stars is, however, very similar, and a single isochrone, corresponding to an age of about 3.5 ± 0.5 Myr, reproduces most of the single and binary O star population in NGC 6231.

The age obtained from evolutionary tracks that incorporate initial stellar rotation is, however, somewhat different in both sets of models. The Ekström et al. (2012) rotating models adopt an initial $v_{\rm eq}$ of $0.4 v_{\rm crit}$, which is of the order of 200–220 km s^{-1} for the mass range considered. Figure 15 (right panel) compares the Ekström et al. and Brott et al. models with similar initial rotation rates. For the Brott et al. models, the location of the isochrones is little affected and our previous age estimates stand. However, the Ekström et al. rotating isochrones are shifted to higher temperatures so older isochrones, of 4–7 Myr, are needed to reproduce the HRD position of the NGC 6231 O-type stars. One has to adopt an initial rotation larger than 400 km s^{-1} for the Brott et al. models to fit a similar cluster age. Such a large initial rotation is unlikely, however, given that the majority of unevolved O-type stars are relatively slow rotators (e.g., Penny & Gies 2009).

The question of whether the formation of high-mass stars in a star-forming region triggers or suppresses the formation of lower mass stars (see, e.g., Herbig 1962) can in principle be tested by comparing the age of the high- and low-mass stellar population in NGC 6231. Unfortunately, uncertainties in the evolutionary calibrations make it difficult to age-date the high-mass stars with sufficient confidence.

If the bulk of the NGC 6231 high-mass stars are truly 5 or 6 Myr old, they would be born at the very beginning of the star-forming event that lead to the formation of NGC 6231. On the other hand, an age of 3.5 ± 0.5 Myr old would see them formed when star formation activity was at its peak (see Figure 11).

5.3. Primordial Mass Segregation or Dynamical Evolution

The current theoretical point of view on mass segregation in young open clusters is that it results from the rapid dynamical

evolution of clumps in the subvirial state (McMillan et al. 2007; Allison et al. 2009b). This picture implies that there should be several clumps in a star-forming region, and that the star-forming region may be, on average, less dense than the case of only a single star-forming clump in a star-forming region. This means that massive stars could be formed in the peripheral region of a star-forming region. In this case, we could have a chance to observe the formation process of massive stars with masses over 30 $M_\odot$, which would be extremely important, as we still have no detailed information on the formation processes of massive stars.

The surface density profiles and the radial variation of the IMF show clearly that NGC 6231 is mass segregated. And the age of NGC 6231 is much older than the time required for mass segregation in a subvirial cluster with substructure (see Figure 2 of Allison et al. 2009b). So, is the mass segregation in NGC 6231 of dynamical origin? Other types of data can help us decide. The binary fraction of massive O-type stars in NGC 6231 (Sana et al. 2008) is 100% at the center, and it reaches about 60% from 2′ up to 15′ (Sco OB1 region). The mass of a binary system is more massive than single stars, but the binary fraction of O-type stars is nearly the same, even in the peripheral region of NGC 6231. This fact implies that the mass segregation in NGC 6231 may be of primordial origin rather than the dynamical evolution scenario of McMillan et al. (2007) and Allison et al. (2009b).

6. SUMMARY

New wide-field photometry for the young open cluster NGC 6231 is presented and analyzed. The main results obtained from this study are summarized as follows.

1. The reddening law toward NGC 6231 was derived from color excess ratios from the optical to mid-IR *Spitzer*/IRAC bands. The reddening law was slightly higher ($R_V = 3.2$), but very close to the normal reddening law. Interestingly, stars in the cluster center show relatively larger color excess ratios. This fact, and the relatively smaller reddening in the center, are conjectured as the result of strong stellar winds from massive stars or a supernova that exploded a few Myr ago.
2. The IMF and age of NGC 6231 were derived. The age of NGC 6231 is 4–7 Myr ($\Delta\tau_{\rm MS} = 3$ Myr) for massive stars, and 1–7 Myr ($\Delta\tau_{\rm PMS} = 6$ Myr) for low-mass PMS stars using a new stellar evolution models with rotation (Ekström et al. 2012) and by adopting new spectral-type–temperature relation of O-type stars (Martins et al. 2005). The slope of the IMF is slightly shallow, but very close to the Salpeter value ($\Gamma = -1.1 \pm 0.1$). In addition, the total mass of NGC 6231 is estimated to be about $2.6(\pm 0.6) \times 10^3\ M_\odot$ from simulated model clusters using a Monte Carlo method.
3. The surface density profiles of four mass groups were derived. Although there was a large difference in the ratio of central density to field density, the four groups showed similar cluster radii. In addition, the radial variation of the mass function was derived and showed an evident mass segregation in NGC 6231. The mass segregation of massive stars ($m \gtrsim 8\ M_\odot$) was also confirmed from the higher value of the mass segregation ratio $\Lambda_{\rm MSR}$ from the minimum spanning tree. The mass segregation in NGC 6231 may be of primordial origin and not as a result of dynamical evolution because of the constancy of the binary fraction of massive O-type stars with radius.
4. The runaway O-type supergiant HD 153919 could have originated from NGC 6231. Using the *Hipparcos* proper motion data, the past supernova, if it exploded at the center of the polarization (Feinstein et al. 2003), would have exploded about 3.1 Myr ago, and the initial mass of the supernova progenitor is estimated to be 85 $M_\odot$ or higher.

The authors thank the anonymous referee for many insightful comments. H. Sung acknowledges the support of the National Research Foundation of Korea (NRF) funded by the Korea Government (MEST, grant No. 20120005318). H. Sung expresses his thanks to Professor Harvey Butcher, the director of Research School of Astronomy and Astrophysics, ANU for hosting him as a Visiting Fellow.

REFERENCES

Allison, R. J., Goodwin, S. P., Parker, R. J., et al. 2009a, MNRAS, 395, 1449
Allison, R. J., Goodwin, S. P., Parker, R. J., et al. 2009b, ApJL, 700, 99
Allison, R. J., Goodwin, S. P., Parker, R. J., Portegies Zwart, S. F., & de Grijs, R. 2010, MNRAS, 407, 1098
Ankay, A., Kaper, L., de Bruijne, J. H. J., et al. 2001, A&A, 370, 170
Baraffe, I., Chabrier, G., Allard, F., & Hauschildt, P. H. 1998, A&A, 337, 403
Baume, G., Vázquez,, & Feinstein, A. 1999, A&AS, 137, 233
Bessell, M. S. 1995, in Proc. ESO Workshop, The Bottom of the Main Sequence and Beyond, ed. C. G. Tinney (Berlin: Springer), 123
Bessell, M. S., Castelli, F., & Plez, B. 1998, A&A, 333, 231
Bessell, M. S., Peterson, B. A., Wickramasinghe, D. T., & Vidal, N. V. 1974, ApJ, 187, 355
Black, D. T. R., Bode, M. F., Stephenson, F. R., Abbott, T., & Page, K. L. 2008, in ASP Conf. Ser. 401, RS Ophiuchi (2006) and the Recurrent Nova Phenomenon, ed. A. Evans, M. F. Bode, T. J. O'Brien, & M. J. Darnley (San Francisco, CA: ASP), 351
Bok, B. J., Bok, P. F., & Graham, J. A. 1966, MNRAS, 131, 247
Brott, I., de Mink, S. E., Cantiello, M., et al. 2011, A&A, 530, 115
Crowther, P. A. 1997, in IAU Symp. 189, Fundamental Stellar Properties: The Interaction between Observation and Theory, ed. T. R. Bedding, A. J. Booth, & J. Davis (Dordrecht: Kluwer), 137
Damiani, F., Micela, G., Sciortino, S., & Harnden, F. R. 2009, in AIP Conf. Proc. 1094, Cool Stars, Stellar Systems and the Sun (Melville, NY: AIP), 916
Ekström, S., Georgy, C., Eggenberger, P., et al. 2012, A&A, 537, 146
Elson, R. A., Fall, S. M., & Freeman, K. 1987, ApJ, 323, 54
Fazio, G. G., Hora, J. L., Allen, L. E., et al. 2004, ApJS, 154, 10
Feinstein, A., & Ferrer, O. E. 1968, PASP, 80, 410
Feinstein, C., Martínez, R., Marcela Vergne, M., Baume, G., & Vázquez, R. 2003, ApJ, 598, 349
Fitzpatrick, E. L., & Massa, D. 2009, ApJ, 699, 1209
Fryer, C. L., Heger, A., Langer, N., & Wellstein, S. 2002, ApJ, 578, 335
Garrison, R. F., & Schild, R. F. 1979, AJ, 84, 1020
Guetter, H. H., & Vrba, F. J. 1989, AJ, 98, 611
Henize, K. G. 1976, ApJS, 30, 491
Herbig, G. H. 1962, ApJ, 135, 736
Heske, A., & Wendker, H. J. 1984, A&AS, 57, 205
Hill, G. M., Moffat, A. F. J., St-Louis, N., & Bartzakos, P. 2000, MNRAS, 318, 402
Hur, H., Sung, H., & Bessell, M. S. 2012, AJ, 143, 41
King, I. 1962, AJ, 67, 471
Kroupa, P. 2002, Sci, 295, 82
Lim, B., Chun, M.-Y., Sung, H., et al. 2012, AJ, in press (arXiv:1211.5832)
Martins, F., Schaerer, D., & Hillier, D. J. 2005, A&A, 436, 1049
McMillan, S. L. W., Vesperini, E., & Portegies Zwart, S. F. 2007, ApJL, 655, 45
Moeckel, N., & Bonnell, I. A. 2009, MNRAS, 396, 1864
Meynet, G., & Maeder, A. 2000, A&A, 361, 101
Park, B.-G., & Sung, H. 2002, AJ, 123, 892
Penny, L. R., & Gies, D. R. 2009, ApJ, 700, 844
Perry, C. L., Hill, G., Younger, P. F., & Barnes, J. V. 1990, A&AS, 86, 415
Piatti, A. E., Clariá, J. J., & Bica, E. 1998, ApJS, 116, 263
Raboud, D. 1996, A&A, 315, 384
Raboud, D., Cramer, N., & Bernasconi, P. A. 1997, A&A, 325, 167
Raboud, D., & Mermilliod, J.-C. 1998, A&A, 333, 897
Sana, H., Antokhina, E., Royer, P., et al. 2005, A&A, 441, 213
Sana, H., de Mink, S. E., de Koter, A., et al. 2012, Sci, 337, 444

Sana, H., Goset, E., Nazé, Y., Rauw, G., & Linder, N. 2008, MNRAS, 386, 447
Sana, H., Goset, E., Rauw, G., Sung, H., & Vreux, J.-M. 2006, A&A, 454, 1047
Sana, H., Momany, Y., Gieles, M., et al. 2010, A&A, 515, A26
Sana, H., Rauw, G., & Goset, E. 2001, A&A, 370, 121
Sana, H., Rauw, G., Sung, H., Goset, E., & Vreux, J.-M. 2007, MNRAS, 377, 945
Schaller, G., Schaerer, D., Meynet, G., & Maeder, A. 1992, A&AS, 96, 269
Schild, R. D., Hiltner, W. A., & Sanduleak, N. 1969, ApJ, 156, 609
Seggewiss, W. 1968, Veröff. Astron. Inst. Univ. Bonn, No. 79
Siess, L., Dufour, E., & Forestini, M. 2000, A&A, 358, 593
Skrutskie, M. F., Cutri, R. M., Stiening, R., et al. 2006, AJ, 131, 1163
Sung, H., & Bessell, M. S. 2000, PASA, 17, 244
Sung, H., & Bessell, M. S. 2004, AJ, 127, 1014
Sung, H., & Bessell, M. S. 2010, AJ, 140, 2070
Sung, H., Bessell, M. S., & Chun, M.-Y. 2004, AJ, 128, 1684
Sung, H., Bessell, M. S., Chun, M.-Y., Karimov, R., & Ibrahimov, M. 2008a, AJ, 135, 441
Sung, H., Bessell, M. S., Lee, H.-W., Kang, Y. H., & Lee, S.-W. 1999, MNRAS, 310, 982
Sung, H., Bessell, M. S., & Lee, S.-W. 1997, AJ, 114, 2644
Sung, H., Bessell, M. S., & Lee, S.-W. 1998, AJ, 115, 734 (SBL98)
Sung, H., Bessell, M. S., & Sana, H. 2008b, JKAS, 41, 1
Sung, H., Chun, M.-Y., & Bessell, M. S. 2000, AJ, 120, 333
Sung, H., Stauffer, J. R., & Bessell, M. S. 2009, AJ, 138, 1116
van Leeuwen, F. 2007, A&A, 474, 653
Weidner, C., Kroupa, P., & Bonnell, I. A. D. 2010, MNRAS, 401, 275
Weidner, C., Kroupa, P., & Maschberger, T. 2009, MNRAS, 393, 663
Wray, J. D. 1966, PhD thesis, Northwestern Univ.